Fuel 115 (2014) 749–757

Contents lists available at ScienceDirect

Fuel

journal homepage: www.elsevier.com/locate/fuel

Biomass torrefaction and CO_2 capture using mining wastes – A new approach for reducing greenhouse gas emissions of co-firing plants

Amin Sarvaramini [a], Gnouyaro P. Assima [a], Georges Beaudoin [a], Faïçal Larachi [b,*]

[a] Department of Chemical Engineering, Université Laval, Québec G1V 0A6, Canada
[b] Department of Geology and Geological Engineering, Université Laval, Québec, QC G1V 0A6, Canada

HIGHLIGHTS

- CO_2 produced during dry and ionic liquid assisted birch torrefaction is monitored.
- Torrefaction was combined with ultramafic mining residues to capture emitted CO_2.
- Presence of CH_4 and CO in the torrefaction gas did not affect the carbonation rate.
- Native brucite content of mining residues broadly dictated the carbonation rate.
- Effect of temperature and residue pore water on the carbonation rate was studied.

GRAPHICAL ABSTRACT

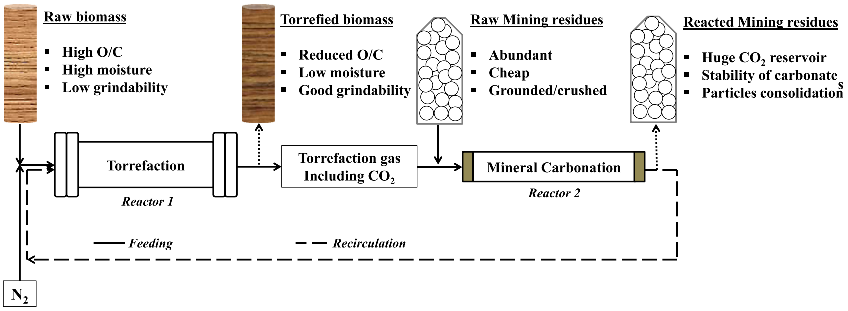

ARTICLE INFO

Article history:
Received 7 June 2013
Received in revised form 21 July 2013
Accepted 23 July 2013
Available online 8 August 2013

Keywords:
Biomass
Torrefaction
Carbon dioxide
Sequestration
Mining residues

ABSTRACT

A novel combination of biomass torrefaction and CO_2 sequestration was explored in which carbonation of mining residues was conducted near ambient temperatures. We report that CO_2 as one of the main gases evolved during torrefaction of lignocellulosic biomass can be trapped using cheap, abundant and already size-reduced mining residues resulting in a carbon-negative torrefaction process. Functionalities of torrefaction as a prerequisite step for an efficient biomass/coal co-firing could thus be further enhanced by curbing the overall process CO_2 emissions. To test this concept, two different Mg-rich ultramafic mining wastes were loaded in a carbonation reactor hyphenated downstream of a torrefaction reactor and operated under total gas reflux to capture the incipient CO_2. The torrefaction unit was operated with birch wood according to conventional dry torrefaction as well as using ionic-liquid-impregnated torrefaction to increase birch wood constituents' torrefaction rate. The effect of some important parameters such as carbonation temperature, residue pore water saturation, and carbon monoxide and methane concentrations on mining residues CO_2 uptake was studied systematically to assess if such a tandem concept would enable displacement and storage of sizeable amounts of CO_2 emitted by torrefaction.

© 2013 Elsevier Ltd. All rights reserved.

1. Introduction

Coal combustion for electricity generation is regarded as one of the most significant sources of greenhouse gas emissions [1]. In 2010, *ca.* 46% of world's electricity demand was generated from coal combustors while coal-based plants contributed *ca.* 70% of CO_2 emissions [2]. In Canada, nearly 80% of CO_2 emissions related to electricity generation (11.5% of Canada's total CO_2 emissions) are ascribed to coal-fired plants [3]. Fractional substitution of coal with biomass as a renewable energy source, i.e., normally viewed as CO_2 neutral in energy conversion systems, is an appealing option to curb CO_2 emissions [4]. In this regard, biomass co-firing with coal is contemplated as a realistic option to alleviate the incidence

---

[*] Corresponding author.
E-mail address: faical.larachi@gch.ulaval.ca (F. Larachi).

0016-2361/$ - see front matter © 2013 Elsevier Ltd. All rights reserved.
http://dx.doi.org/10.1016/j.fuel.2013.07.087

of coal in electricity generation in existing coal-fired plants while requiring small capital investments for retrofitting [5]. In addition to the decrease in coal consumption, co-firing is anticipated to mitigate NO_x and SO_2 emissions thus presenting biomass as a sustainable candidate source for electricity production [6–8]. Efficient and economic coal/biomass co-firing for energy production is hampered by the limited biomass energy contribution which is less than 10% in the majority of currently operated co-firing plants [9]. The most common hurdles are (though not limited to): (1) low energy density of biomass (as compared to coal) due to the large moisture and oxygen contents cause flame instabilities in the combustion chambers [6], (2) low biomass flowability and fluidization properties leading to difficulties in feeding biomass into combustors [10], (3) rigidity and mechanical strength of biomass structure attributed to the long crystalline cellulose fibers intertwined with non-crystalline hemicellulose resulting in higher grinding energy requirements and reducing grinding efficiency of coal-biomass feeds [11].

Torrefaction as a pretreatment technique is proposed as a retrofit measure to alter biomass properties and accommodate its application in co-firing plants [10]. Torrefaction consists of a mild pyrolysis of biomass at temperatures below 300 °C in an oxygen-deprived headspace. Torrefaction, being a thermal O-removal process, increases energy density of treated biomass to achieve heating values nearing those of coal [11–13]. Furthermore, torrefaction promotes partial depolymerization/decomposition of cellulose and hemicellulose. This contributes to reduce fibers length and mechanical stability hence ameliorating biomass grindability properties [10,14,15]. Furthermore, torrefied biomass exhibits more uniform physicochemical properties, e.g., superior flowability and fluidization properties than raw biomass, making it more amenable for co-firing [10,16]. Different torrefaction processes, e.g., dry torrefaction [12,17,18], wet torrefaction [19,20] and ionic-liquid (IL) assisted torrefaction [21] have been investigated to enhance biomass properties. Decomposition of hemicellulose, cellulose and lignin fractions of biomass subjected to above torrefaction processes could release some low calorific-value gases such as carbon dioxide, water and some types of organic acids, such as formic and acetic acids [22]. Depending on the type of biomass and torrefaction conditions (temperature and treatment time), up to 30% of carbon can be released in the form of CO_2 [22].

Although biomass is a CO_2-neutral source of energy, a torrefaction process hyphenated with capture of its evolved CO_2 gas could constitute an appealing option for co-firing plants to reduce their net CO_2 emissions. Furthermore, due to the importance of mitigating CO_2 emissions into the atmosphere, recent studies predict that the net negative greenhouse gas emissions from bioenergy with carbon capture and storage plants could be as much as 10^9 metric tons of CO_2 per year near 2050. This emphasizes the importance of intercepting CO_2 streams in future bioenergy-based plants [23]. In this regard, a combined continuous torrefaction and carbonation process is investigated in this study for trapping the CO_2 formed during torrefaction as a negative net CO_2 emission torrefaction process. The proposed CO_2 trapping process is based on the carbonation at nearly ambient temperature and pressure of cheap, easily-accessible, already-mined and pre-ground ore residues and tailings [24–27]. In particular, those consisting of mafic/ultramafic mining wastes, due to their high Mg content (up to 20 wt.%), are known to be very reactive with CO_2 [28]. Recently, our group studied the ability of ultramafic mining residues to directly capture CO_2 under ambient conditions and outlined the enhanced rate of carbonation under anoxic and low liquid saturation environments [29,30]. The carbonation reactions led to the formation of stable carbonate minerals such as nesquehonite and dypingite [30]. These findings suggest a possibility to combine biomass torrefaction with CO_2 fixation and whereby CO_2 produced during torrefaction could be trapped over moistened mining residues. The fact that the entire chain proceeds anoxically is also advantageous for the carbonation of residues as their carbonation activity was shown to decay in the presence of oxygen [29].

To study the possibility of on-stream biomass torrefaction and carbonation of mining residues, an assembly consisting of a hyphenated torrefaction–carbonation reactor was designed. The carbonation potential of two types of ultramafic tailing residues was assessed by testing streams of CO_2 produced during dry and ionic-liquid torrefaction of birch wood. The study's aim specifically addressed the impact of carbonation temperature, residues pore water saturation, and CO and methane composition of the evolving torrefaction gas on the carbonation rate of the mining residues.

2. Experimental

2.1. Materials preparation

To investigate the potential of ultramafic mining residues for capturing CO_2 from a torrefaction gas, two samples were used (1) chrysotile mining residues (CMR) received from the Black Lake Mine tailings (Thetford Mines, Québec, Canada) and (2) nickel mine residues (NMR) obtained from the exit of the defibering process of Royal Nickel Corporation's Dumont Nickel project pilot plant (Amos, Québec, Canada). The samples received were in two separate sealed 25 L containers to avoid contact of the residues with air during their transportations. The mining residue samples were then sieved to isolate particles smaller than 1.5 mm to be used for the carbonation experiments. Powder X-ray diffraction analysis of the two samples revealed the presence of chrysotile and lizardite as major minerals along with minor components such as magnetite, brucite, albite, chlorite, talc, phlogopite and wustite. The native brucite content, one of the active minerals for carbonation, was *ca.* 2.94 wt% and 10.9 wt% in CMR and NMR, respectively. Detailed information about these residues is available elsewhere [29,30]. Prior to experiments, the (porous) residue samples were moistened with water to achieve up to *ca.* 50% liquid saturation.

Isothermal torrefaction studies were performed using birch, an abundant wood biomass source from Québec forests. Before the experiments, the as-received tiny sheets of birch wood (bark-freed) samples were cut into small pieces to obtain woodchips in the 2–4 mm size range. The proximate analysis of birch wood showed the presence of 5.5% of humidity. The volatiles, fixed carbon and ash content of the samples were 89.4%, 9.8% and 0.7% on a dry basis, respectively. The same batch of birch wood is used for all the torrefaction experiments performed in this study and the CHNS analysis performed on the samples proved the homogeneity of the birch wood samples. Birch wood torrefaction was performed using two different processes. In the first series of experiments, non-pretreated birch samples were torrefied at 260 °C for 60 min, referred here to as dry torrefaction. At 260 °C, all the biomass constituents such as hemicellulose, cellulose and lignin are torrefied leading to an appropriate estimation of CO_2 production from the birch torrefaction. The rate of biomass torrefaction at 260 °C is not very high leading to a good control over the torrefaction experiments and their repeatability in terms of torrefaction mass yield and CO_2 production rate during torrefaction. In a second series, birch wood samples were impregnated with 1-ethyl-3-methyl imidazolium trifluoromethanesulfonate ionic liquid (IL) at 60 °C ([Emim][OTf], Sigma Aldrich, purity > 98 %.) and then torrefied at 260 °C for 30 min. Impregnation of biomass with ionic liquids has been shown to enhance the rate of cellulose torrefaction at temperatures lower than 300 °C [21]. Consequently, the torrefaction of IL-impregnated birch wood was carried out to evaluate the extent of carbon dioxide production associated with this process. The final mass ratio of absorbed IL to birch was around 2.

2.2. Experimental assembly

The biomass samples were torrefied in a fixed-bed reactor (Fig. 1). The bench scale biomass torrefaction unit consisted of a stainless steel fixed-bed reactor (internal diameter 0.34 cm, length 70 cm) placed inside an induction coil. For each experiment, one gram of dry or IL-impregnated biomass sample was held atop of a steel grid located in the middle of a stainless steel tube to act as a support for the biomass bed. The reactor was heated through a 30 cm long coil connected to a 18 kW induction power supply for heating the stainless steel tube *via* an AC magnetic field then heating in turn the biomass layer through radiation and conduction. The biomass bed temperature was raised from the ambient to a target temperature of 260 ± 0.1 °C and kept there for specified time durations.

The gas exiting from the torrefaction reactor was directed towards the top of a carbonation reactor (cylindrical tube, 5.8 cm internal diameter) where carbonation took place through a 1.2 cm thick layer of mining residues. The carbonation column consisted of two compartments: an upper headspace occupying *ca.* 75% of the column volume, the mining residue bed and a lower compartment. The CO_2 concentration, gas humidity and temperature in upper compartment were measured with CO_2 sensors (GMT221 CO_2 transmitter display 0–10%, Vaisala) and integrated hygrometer-thermocouples (HMT333 moisture-temperature transmitter, Vaisala). To homogenize the gas composition in both upper and lower compartments, each was gently mixed with a dedicated electrical fan. The bed characteristics, i.e., its temperature, pore water pH and ionic conductivity during carbonation were also monitored as a function of time. A multi-task time-domain reflectometer (TDR) probe (DELTA-T WET-2-K1, Hoskin Scientific) was inserted laterally in the residue layer for on-line monitoring of liquid saturation, bulk ionic conductivity (of solid, extra- and intra-porous water) and bed temperature. A pH probe (8616AQ, Hanna instruments) was also used to register the instantaneous residue pore-water pH.

The gas exiting the bottom of the carbonation column was recirculated to the torrefaction reactor by means of a peristaltic pump (Fig. 1). Due to the slow reaction rates of both torrefaction and mineral carbonation reactions, the torrefaction gas was circulated between the two reactors to provide longer contact times between mining residues and CO_2 to enable its fixation. Before entering the torrefaction reactor, a sample of gas was taken by an Agilent micro-GC 3000 to quantify the concentrations of CO, CH_4, H_2 and CO_2. To start-up the tandem torrefaction–carbonation, biomass and water partially-saturated (50%) mining residue samples were first loaded in the torrefaction and carbonation reactors, respectively. Afterwards, the whole assembly was purged under nitrogen stream (1 L/min) to remove pre-existing oxygen and carbon dioxide. Once micro-GC and CO_2 probe O_2 and CO_2 signals were below detection limits, gas circulation and torrefaction reactor heat-up were initiated.

After test completion, the torrefied birch wood removed from the steel grid was dried at 110 °C. In the case of IL-impregnated birch wood, the solid biomass was first mixed with water and immersed in an ultrasound bath at 60 °C to separate IL from birch wood. The samples then were placed on a filter paper and washed with approximately 200 mL of distilled water using vacuum filtration. The solid recovered was dried in an oven at 110 °C. The solid

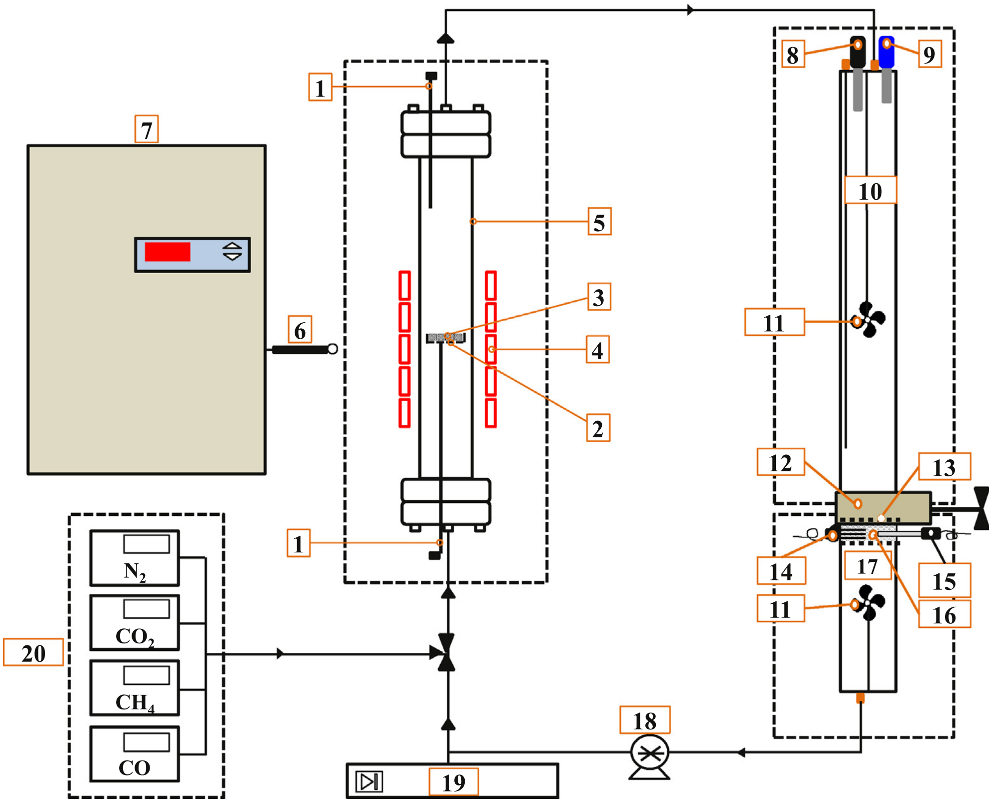

Fig. 1. Schematic of experimental torrefaction-carbonation assembly. (1) K-type thermocouple, (2) stainless steel mesh, (3) birch sample holder, (4) induction coil, (5) stainless steel torrefaction reactor, (6) pyrometer, (7) induction power supply, (8) CO_2 probe, (9) hygrometer-thermocouple, (10) carbonation upper compartment, (11) electrical fan, (12) gate, (13) stainless steel filter, (14) TDR probe, (15) pH probe, (16) residue bed holder, (17) carbonation lower compartment, (18) peristaltic pump, (19) micro-GC and (20) mass flowmeters.

products obtained after torrefaction were analyzed to quantify their properties after thermal treatment. The solid products were weighed to obtain their mass yield (Y_M = %mass solid product/mass feed) after torrefaction. The C, H, N, S contents of the samples were also measured using an elemental analyzer (Fisons EA 1108CHNS). All measurements were repeated twice and their averages were reported. The higher heating value (HHV) of the samples before and after torrefaction were determined using a relationship based on carbon, hydrogen, oxygen, sulfur, nitrogen and ash content of biomass suggested by Channiwala et al. [31], where

$$\text{HHV (kJ/g)} = 0.3491 \times \text{C} + 1.1783 \times \text{H} + 0.1005 \times \text{S-}0.1034 \times \text{O-}0.0151 \times \text{N-}0.0211 \times \text{Ash}$$

With C, H, S, O, N and Ash representing carbon, hydrogen, sulfur, oxygen, nitrogen and ash mass percentages, respectively. Using the solid product HHV, the energy density (e = HHV solid product/HHV feed) and energy yield ($Y_e = e \cdot Y_M$) of the solids were also obtained. To investigate the effect of torrefaction on the samples hydrophobicity, equilibrium moisture content (EMC) analysis was also performed on the torrefied samples. EMC of raw and torrefied biomass samples were obtained by putting 300 mg samples in a vapor-saturated environment controlled at 25 °C.

3. Results and discussion

3.1. Analysis of torrefaction products

To determine the extent of torrefaction, the solid torrefaction products were thoroughly analyzed. The mass yield of solid products of the IL and dry torrefied birch were 73.2% and 75.1 %, respectively, which lie within the expected range for torrefaction (Table 1). Due to the considerably accelerated [Emim][OTf]-mediated torrefaction rate resulting in a lower mass yield of torrefied solid product, IL-impregnated birch was torrefied for a shorter time (30 min) compared to its dry torrefaction (60 min). As seen in Table 1, both IL-impregnated and dry-treated torrefied birch exhibited increased HHV showing improvements in birch energy density after torrefaction. The carbon content in the as-received birch (47.9 wt%) increased to 51.8 wt% and 48.8 wt% for dry and IL-impregnated torrefied sample, respectively (Table 1). Also, the carbon content of dry-torrefied birch exceeded that of IL-impregnated birch. Detection of 0.5 wt% of sulfur in the washed and dried IL-torrefied birch samples indicated that nearly 4 wt% of IL resisted the washing step and kept trapped inside the solid structure of the torrefied product. IL leftover in the torrefied birch reduces its HHV since [Emim][OTf] carbon represents 32.3%. Resting the IL carbon contribution from that of IL-torrefied birch boosts torrefied birch carbon content to 49.5 wt% which is still lower than that of dry torrefied birch. IL-impregnated torrefied wood had considerably higher rates of decomposition though this was counterbalanced by a slight loss in quality of torrefied solid product in comparison to classical dry torrefaction. The EMC values of IL-impregnated and dry torrefied birch were, respectively, 30% and 40% lower as compared to as-received birch. The slightly higher moisture uptake of IL-treated birch was due to the [Emim][OTf] hydrophilic nature possibly compensating for the breakage of hydroxyl groups which promote hydrophobic surface during torrefaction [32].

Table 1
Ultimate analysis, mass yield, higher heating value and energy yield of as- received and torrefied birch.

Samples	C (wt%)	H (wt%)	N (wt%)	S (wt%)	O (wt%)	Ash (wt%)	Mass yield (Y_M, %)	Energy yield ($Y_{e,\%}$)	HHV (kJ/g)
As received birch	47.9	6.1	0.02	0	45.3	0.7	–	100	19.2
Dry torrefied	51.8	6.03	0.14	0	41.2	0.8	75.1	81.7	20.9
[Emim][OTf] torrefied	48.8	6.1	0.37	0.5	42.8	0.5	73.2	75.4	19.8

3.2. Carbonation-free torrefaction

Two blank experiments were performed in the torrefaction-carbonation assembly to monitor the concentrations of CO_2, CO, CH_4 and H_2 produced during dry torrefaction and IL-impregnated torrefaction of 1 g of birch in the absence of mining residues.

CO_2 concentration during dry torrefaction of birch increased over time leading to its build-up in the setup as measured in upper and lower carbonation compartments (Fig. 2). Torrefaction at 260 °C featured an early fast CO_2 production lasting 20 min where 58% of CO_2 was produced. Fast hemicellulose decomposition starting at near 220 °C, was likely the cause of such considerable CO_2 release in the first 20 min of torrefaction [33,34]. However, cellulose and lignin are also decomposed slowly along with hemicellulose leading to the production of 9×10^{-3} mol/g of CO_2 in 60 min. This amounted only to 16.2% of the carbon lost by birch during dry torrefaction. Besides carbon dioxide, carbon release also took place in the form of condensable hydrocarbons, e.g., acid formic and acetic, [22] CO and CH_4. The rate of CO production was almost constant during blank test torrefaction (Fig. 3a) and its amount at the end of torrefaction contributed 40% of that of carbon dioxide (0.33×10^{-3} mol/g; Fig. 3c). Dry torrefaction also led to the production of a small amount of methane (0.015×10^{-3} mol/g) while no hydrogen production was detected.

The profile of carbon dioxide production during the blank experiment of [Emim][OTf] impregnated birch torrefaction is presented in Fig. 4. Torrefaction was performed at 260 °C for the duration of 30 min. Torrefaction of IL-impregnated birch also showed a fast release of carbon dioxide over the first 10 min followed by a gentler rate up to 30 min. The rate of cellulose decomposition was stimulated by [Emim][OTf] at 260 °C. This translated into CO_2 production (1.1×10^{-3} mol/g) in 30 min outpacing by 20% that produced in 60 min by birch dry torrefaction. Independent thermal treatments of [Emim][OTf] at [21] 260 °C unveiled neither CO_2 production nor IL thermal degradation confirming that CO_2 produced originated solely from birch decomposition. The release of CO vis-à-vis CO_2 was quite marginal, i.e., 0.19×10^{-3} mol/g (Fig. 3b) which was 47.5% less than that produced during birch dry torrefaction (Fig. 3a). However, the proportional changes in the amounts of CO and CO_2 led to almost constant CO/CO_2 ratio for dry and IL-impregnated torrefaction of birch alike (Fig. 3c and d). Likewise, no methane production was observed during torrefaction of IL-impregnated birch.

3.3. Coupled torrefaction-carbonation

CO_2 evolution in the torrefaction-carbonation assembly after CMR and NMR were loaded in the carbonation reactor and birch dry torrefaction enabled is shown in Fig. 2. Carbonation of CMR and NMR residues started almost 10 min after the onset of torrefaction. Such short delay was attributed to diffusion limitation of CO_2 in the residue pore water before reacting with the leached magnesium. The NMR carbonation rate outpaced that of CMR under identical conditions. The unreacted CO_2 in the presence of NMR peaked around 0.37×10^{-3} mol/g at 25 min of torrefaction. This was almost 36% lower than in the blank carbonation-free experiment demonstrating that both CO_2 production and sequestration were occurring simultaneously. Although CO_2 is still produced in the torrefaction reactor, the rate of carbonation was higher than the rate of CO_2 production leading to the decrease of

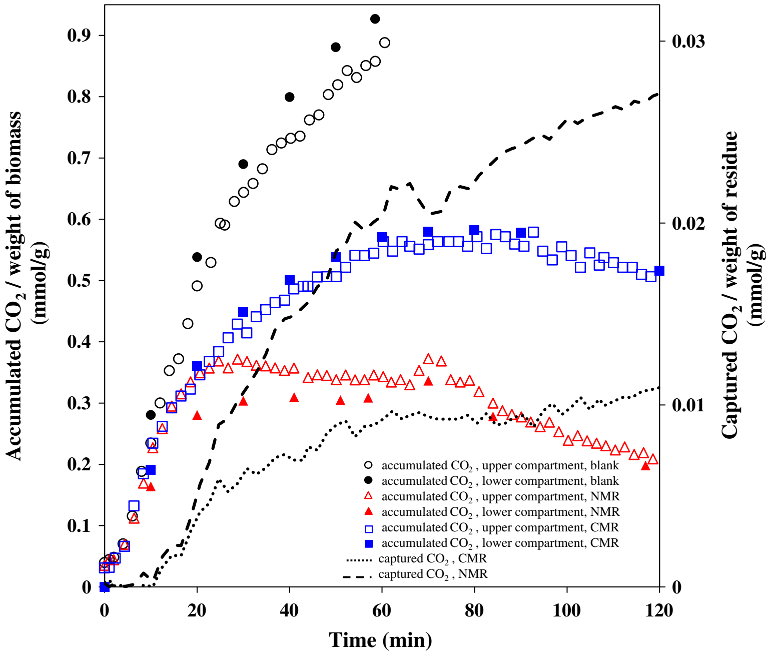

Fig. 2. Time evolution of accumulated (left *y*-scale) and captured (right *y*-scale) CO_2 during birch dry torrefaction at 260 °C. The marginal differences in CO_2 compositions in upper (empty symbols) and lower (filled symbols) compartments is worthy of notice.

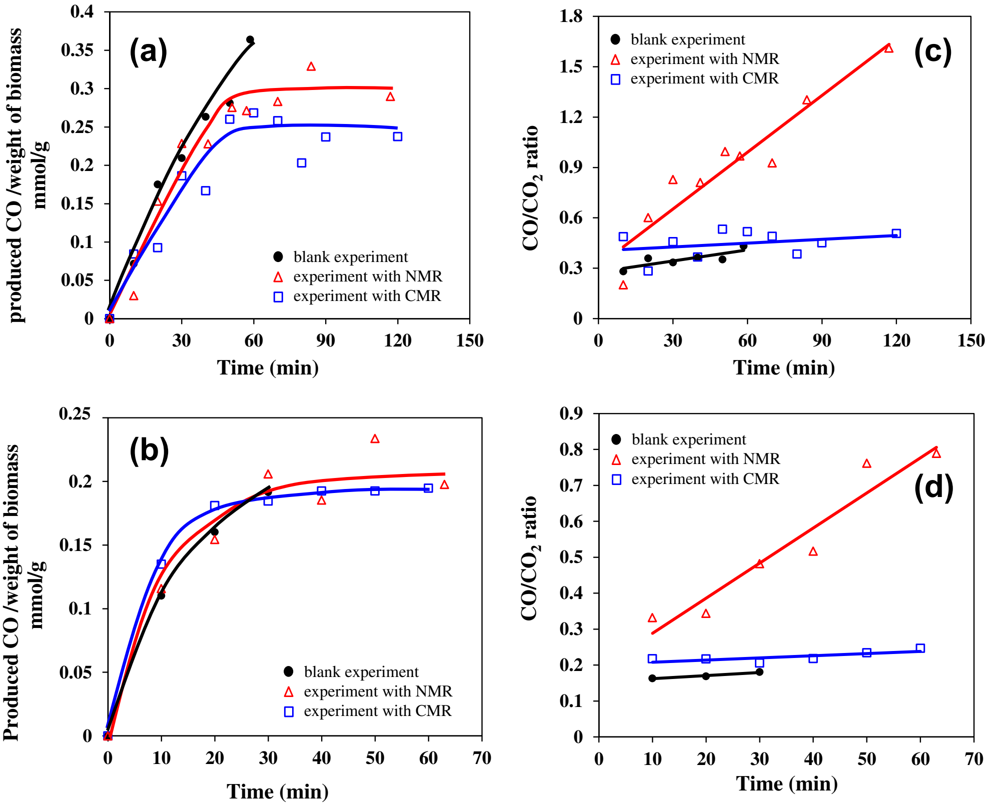

Fig. 3. Time evolution of accumulated CO during (a) dry birch torrefaction, (b) IL-impregnated birch torrefaction. Time evolution of CO/CO_2 mole ratio during (c) dry birch torrefaction and (d) IL-impregnated birch torrefaction.

CO_2 concentration in the tandem assembly. Up to 60 min torrefaction time (Fig. 2), almost 62% of carbon dioxide produced was sequestered within the NMR samples. After this time period, birch torrefaction was suddenly quenched while the gas stream in the assembly was recirculated and depletion of CO_2 solely due to carbonation at ambient temperature was monitored. As seen in Fig. 2, gaseous CO_2 was depleting very fast as no carbon dioxide was coming from the torrefaction reactor. It was estimated that 0.34% of NMR magnesium was carbonated in 2 h to displace 42% of the produced CO_2. The rate of CMR carbonation was slower than

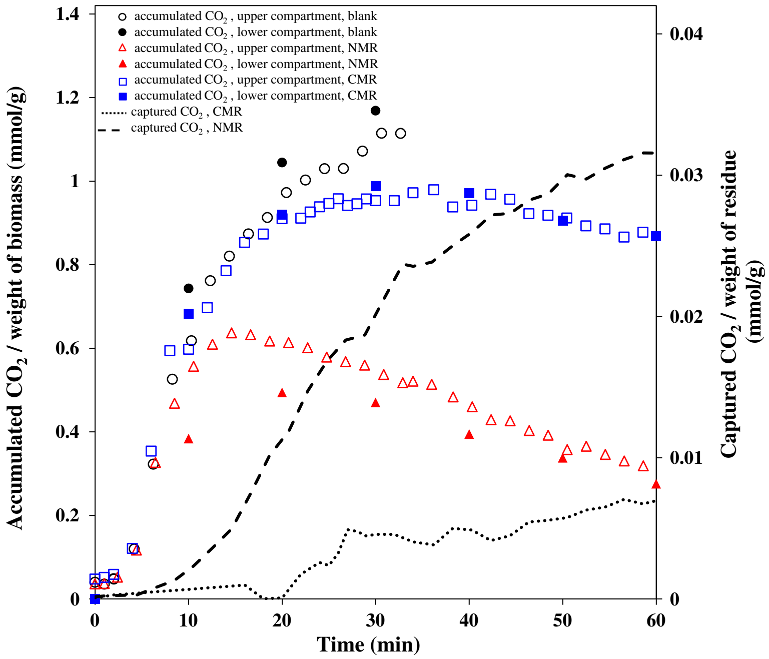

Fig. 4. Time evolution of accumulated (left *y*-scale) and captured (right *y*-scale) CO_2 of the torrefaction of IL-impregnated birch at 260 °C. Differences in CO_2 compositions in upper (empty symbols) and lower (filled symbols) compartments reveal strong carbonation reactivity of residues.

the rate of CO_2 production in the torrefaction reactor. After 60 min torrefaction, CO_2 concentration was 35.9% lower than that in the blank experiment and only 0.17% of CMR magnesium was carbonated in 2 h. Residue carbonation also led to an increase of CO/CO_2 ratio (Fig. 3c) due to both CO_2 sequestration and continuous CO generation (Fig. 3a). The CO/CO_2 ratio obtained using NMR exceeded that obtained with CMR (Fig. 3c).

Carbonation of [Emim][OTf]-torrefied birch in the presence of CMR and NMR is shown in Fig. 4. In these series of experiments, torrefaction lasted 30 min before the torrefaction reactor was quenched keeping gas recirculation for another 30 min NMR and CMR carbonation period. Carbonation of NMR started after 5 min. The large difference between 10 and 30 min in CO_2 concentrations from upper and lower compartments of the carbonation column is an indicator of fast NMR carbonation. CMR carbonation pattern was similar to that observed during birch dry torrefaction. CO_2 accumulated after 30 min of experiment using CMR was 15% lower than that of the blank carbonation-free test. Yet, by letting carbonation to proceed after 30-min torrefaction, the CO_2 content in the assembly was reduced to 0.87×10^{-3} mol/g corresponding to the capture of 22% of the total of CO_2 produced. Magnesium involved in the carbonation reaction using CMR and NMR during IL-torrefaction of birch amounted only to 0.11% and 0.4%, respectively.

A special attention is paid in this study to reduce the experimental errors resulting from the coupling of torrefaction and carbonation reactors. The temperature and residence time of birch wood in the torrefaction reactor was controlled (260 ± 0.1 °C) so that the mass yield of IL assisted and dry-torrefied birch wood samples varied by less than 1% for different experiments. The birch wood samples, all taken from the same batch, exhibited similar CHNS contents and thus highly repeatable torrefaction experiments. The variation in the amount of produced carbon dioxide is also less than 2.5% for the torrefaction experiments repeated at 260 °C for IL assisted and dry-torrefied birch wood samples. Furthermore, although the CMR and NMR samples used at different carbonation experiments were picked from the same batches of residues, the heterogeneity of residues could lead to some differences in their extent of CO_2 sequestration. Assima et al. [29,30] investigated the effect of heterogeneity of CMR and NMR residues on the extent of CO_2 sequestration at different CO_2 concentrations. The carbonation experiments performed with NMR residue showed that this sample heterogeneity could lead to less than 0.6% difference in its extent of CO_2 sequestration. This value was higher for CMR (*ca.* 2.1%).

3.4. Origin of residue carbonation activity

The superior activity of NMR compared to CMR is attributed to the higher content of native brucite in the former [35] (10.9 wt% and 2.94 wt%, respectively). Brucite is dissolving rapidly in the pore water, liberating magnesium ions which were promptly bounded with dissolved CO_2. Chrysotile, and to a lesser extent lizardite, at their contact with water also led to the leaching of additional Mg ions [30]. In the presence of dissolved CO_2 species, the leached Mg is precipitated in the form of magnesium carbonates under alkaline medium according to the following reactions [30]:

$$Mg(OH)_2 + CO_2 \rightarrow MgCO_3 + H_2O$$

$$Mg_xSi_yO_{x+2y-z}(OH)_{2z} + xCO_2 \rightarrow xMgCO_3 + ySiO_2 + zH_2O$$

The initial pH of both NMR and CMR pore water was in the range of 9.5–10 (Fig. 5a and b) due to residue dissolution, and especially brucite, in the pore water. The pH of both media began to drop 5 min after torrefaction was started. The drop in pH of NMR during torrefaction was lower than with of CMR. Also, the pH of NMR reached a plateau in less than 20 min while a steady decrease of pH for CMR was observed during the whole 60 min of torrefaction. This pH decrease is attributed to the dissolution of CO_2 in pore water [29]. The brucite-rich NMR sample led to a less pronounced pH drop since enough brucite was dissolved producing sufficient amount of hydroxide to compensate for the acidity generated by CO_2 dissolution. The contribution of both dissolved and leached ionic species could be also seen through the trend of ionic conductivities shown in Fig. 6a and b. The continuous dissolution of CO_2 as well as Mg leaching led to the observed increase in ionic

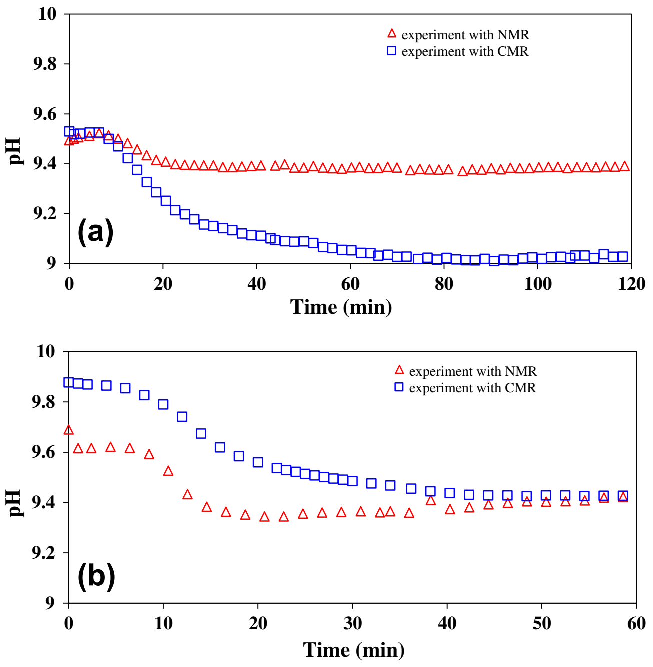

Fig. 5. pH profiles versus time during, (a) dry birch torrefaction and (b) IL-impregnated birch torrefaction.

conductivity of the moistened residues. However, the increase in CMR ionic conductivity exceeded that of NMR. This could be attributed to the higher rate of Mg carbonation with NMR leading to the formation and precipitation of $MgCO_3$ subsequently resulting in less ionic species in NMR pore water than CMR. The unchanged liquid saturation level during carbonation is worthy of notice (Figs. 6a and b).

3.5. *Effect of CO and CH_4 on residue carbonation*

Carbon monoxide and methane built up in the recirculating gas during torrefaction–carbonation. To investigate the effect of increasing CH_4 and CO concentrations on the rate of carbonation, further studies were performed by contacting NMR with two simulated torrefaction gases having different CO and CH_4 contents. In the first experiment, the upper carbonation compartment was filled with a gas mixture composed of 3.23/1.57/0.52 mole% of CO_2, CO and CH_4, respectively in N_2 gas, while the lower compartment was initially purged with pure nitrogen. Another experiment was performed with a mixture richer in CO and CH_4 by filling the upper compartment with a gas mixture consisting composed of 3.13/9.2/3.15 mole% of CO_2, CO and CH_4, respectively in N_2 gas. At $t = 0$, the upper compartment gas contacted with the NMR bed by opening the separation gate (Fig. 1) between the two compartments and recirculating the gas using a peristaltic pump. The CO_2 concentration in the upper and lower compartments was monitored for 1 h using two CO_2 probes. The trend of CO_2 concentration is shown in Fig. 7 where the sequestrated CO_2 was determined by subtracting the instantaneous CO_2 amount from the initial amount of carbon dioxide. As can be observed in Fig. 7, the rate of carbonation within NMR was barely affected by the CO and CH_4 composition in the reacting gas. The difference observed on the amount of carbonation sequestered under various carbon monoxide and methane contents could be attributed to the tiny difference in the initial CO_2 concentration of the reacting gas mixtures [29,30].

3.6. *Effect of temperature on residue carbonation*

The effect of temperature on the rate of carbonation was also investigated. Nearly 8 g of pre-watered NMR samples (liquid saturation = 50%) was placed on a steel mesh and the torrefaction gas was passed through the residue bed. The torrefaction gas was produced by dry torrefaction of one gram of birch samples for 60 min

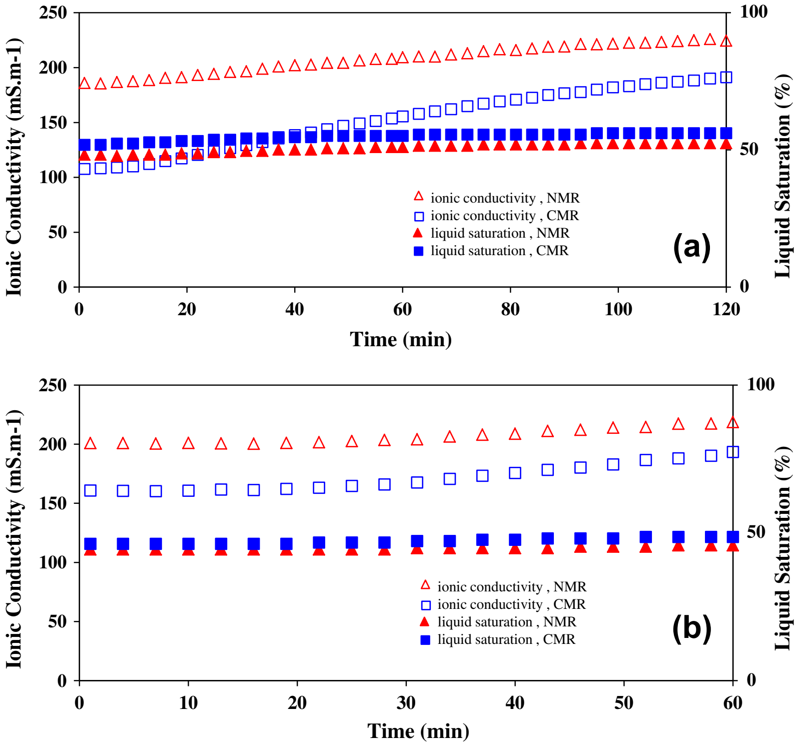

Fig. 6. Profiles of ionic conductivity and liquid saturation versus time during, (a) dry birch torrefaction and (b) IL-impregnated birch torrefaction.

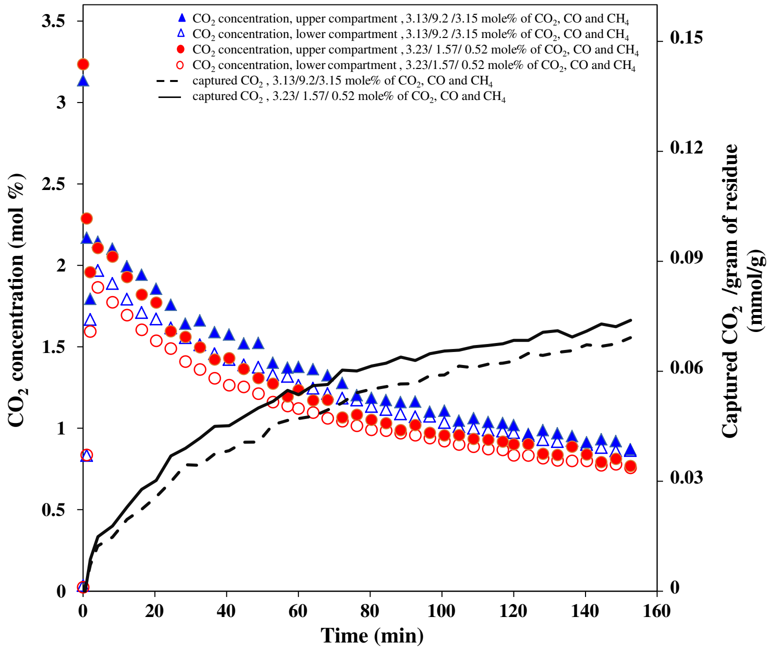

Fig. 7. Effect of CO and methane content on CO_2 instantaneous concentration and amount of captured CO_2 using NMR.

and NMR carbonation was carried out at three different temperatures of 25 °C, 45 °C and 65 °C. Blank experiments performed without NMR residue showed production of *ca.* 0.95 × 10^{-3} mol of CO_2 after 60 min of dry torrefaction (Fig. 8). NMR carbonation at 25 °C reduced considerably the amount of CO_2 in the assembly during torrefaction. At the end of torrefaction, the amount of CO_2 accumulated in the assembly was 0.59 × 10^{-3} mol, a reduction of 38% in the amount of accumulated CO_2 corresponding to almost 0.70% of carbonated Mg at 25 °C. Carbonation at 45 °C lowered CO_2 accumulated to 0.43 × 10^{-3} mol after 60 min (Fig. 8) corresponding to carbonation of almost 55% of carbon dioxide produced during torrefaction and 0.93% of residue Mg. Increasing temperature to 65 °C did not translate into significant gain in the extent of carbonation with a final accumulated CO_2 in the assembly equal to 0.45 × 10^{-3} mol. The amount of pore water of NMR sample after 1 h of carbonation at 65 °C was reduced by 65% while carbonation at 45 °C resulted in the evaporation of only 20% of pore water. Evaporation and reduction of the amount of leached Mg at 65 °C could be a reasonable explanation to the limited observed carbonation reactivity. The importance of pore water on carbonation was therefore investigated by performing carbonation tests at 45 °C without adding at all water to the NMR at the beginning of carbonation test. The rate of carbonation was considerably lower for the dry NMR at 45 °C (Fig. 8). The accumulated carbon dioxide in the

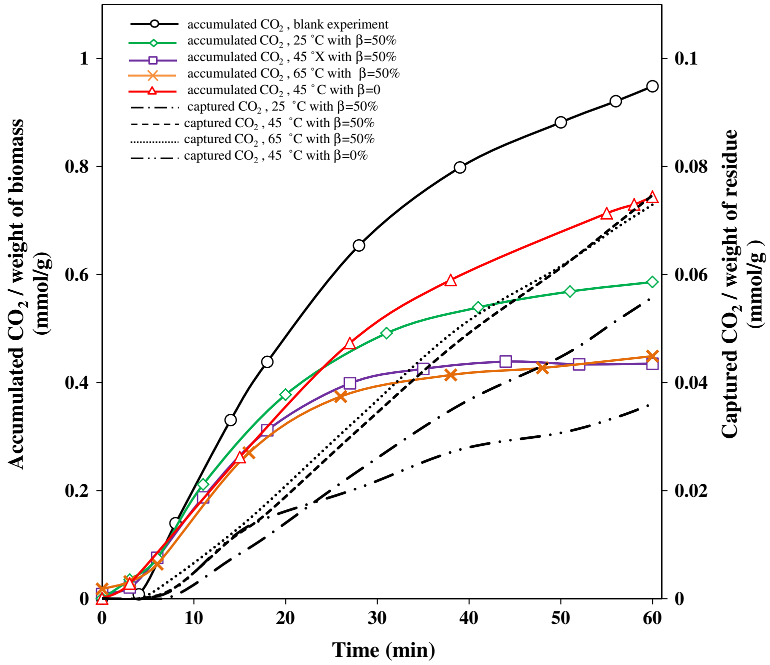

Fig. 8. Effect of temperature on accumulated and captured CO_2 versus time during dry birch torrefaction in the presence of NMR (liquid saturation, β = 50%).

assembly was around 0.74×10^{-3} mol and was considerably higher than that when the residue was moistened at 50% liquid saturation. The presence of some humidity in the torrefaction gas and consequently capillary condensation of water could lead to the limited Mg and CO_2 dissolution which resulted to the observed low reactivity of the dry NMR samples.

4. Conclusion

The concept of simultaneous torrefaction and CO_2 sequestration using mining residues was investigated in this study. The use of mining residues led to a considerable reduction in the amount of CO_2 produced by torrefaction. Approximately 62% and 22% of the CO_2 emitted was captured with nickel and chrysotile mining residues, respectively. This discrepancy in carbonation was ascribed to the difference in their mineralogical composition, especially their different contents in brucite. The rate of carbonation was also shown to be highly dependent to temperature, residue pore water and CO_2 composition. Increasing carbonation temperature improved significantly CO_2 uptake. However, under elevated carbonation temperatures, a regular watering of mining residues is required to compensate for the evaporated pore water. Furthermore, capturing CO_2 could increase the concentration of reactive non-condensable gases such as CH_4 and CO which could be burned along with the condensable gases for improved process heat integration.

The results obtained in this study showed a good potential for combined torrefaction and mineral carbonation suggesting that local torrefaction plants could be built close to mining residue tailings, especially those rich with free brucite, to sequestrate the CO_2 produced from the torrefaction plants. CO_2 sequestration in the local torrefaction plants could partly compensate for the high CO_2 emission from coal combustion. Considering that mining residues are abundant and already crushed, they could represent a cheap solution for CO_2 sequestration. Bearing in mind that the torrefaction process is performed at 200–300 °C, the required energy for heating the mining residues to 40–50 °C (to stimulate the carbonation rates) could also be provided by the flue gas generated in the torrefaction plant. The torrefied biomass in the local torrefaction plants could be then pelletized and transported to co-firing plants for further mixing with coal in combustors.

Acknowledgments

Support from the Natural Sciences and Engineering Research Council of Canada, the Canada Research Chair “Green processes for cleaner and sustainable energy”, and the FQRNT-funded “Center in Green Chemistry & Catalysis” (CGCC) is gratefully acknowledged.

References

[1] Roy J, Sarkar P, Biswas S, Choudhury A. Predictive equations for CO_2 emission factors for coal combustion, their applicability in a thermal power plant and subsequent assessment of uncertainty in CO_2 estimation. Fuel 2009;88:792–8.
[2] The outlook for energy: a view to 2040, 2013. <www.exxonmobil.com/energyoutlook>.
[3] Canada’s emissions trends 2012. Environment Canada; 2012.
[4] McIlveen-Wright DR, Huang Y, Rezvani S, Mondol JD, Redpath D, Anderson M, et al. A techno-economic assessment of the reduction of carbon dioxide emissions through the use of biomass co-combustion. Fuel 2011;90:11–8.
[5] Tillman DA. Biomass cofiring: the technology, the experience, the combustion consequences. Biomass Bioenergy 2000;19:365–84.
[6] Sami M, Annamalai K, Wooldridge M. Co-firing of coal and biomass fuel blends. Prog Energ Combd Sci 2001;27:171–214.
[7] Demirbas A. Sustainable cofiring of biomass with coal. Energy Conv Manage 2003;44:1465–79.
[8] Li J, Yang WH, Blasiak W, Ponzio A. Volumetric combustion of biomass for CO_2 and NO_x reduction in coal-fired boilers. Fuel 2012;102:624–33.
[9] Basu P, Butler J, Leon MA. Biomass co-firing options on the emission reduction and electricity generation costs in coal-fired power plants. Renew Energy 2011;36:282–8.
[10] Li J, Brzdekiewicz A, Yang WH, Blasiak W. Co-firing based on biomass torrefaction in a pulverized coal boiler with aim of 100% fuel switching. Appl Energy 2012;99:344–54.
[11] van der Stelt MJC, Gerhauser H, Kiel JHA, Ptasinski KJ. Biomass upgrading by torrefaction for the production of biofuels: a review. Biomass Bioenergy 2011;35:3748–62.
[12] Medic D, Darr M, Shah A, Potter B, Zimmerman J. Effects of torrefaction process parameters on biomass feedstock upgrading. Fuel 2012;91:147–54.
[13] Uemura Y, Omar WN, Tsutsui T, Yusup SB. Torrefaction of oil palm wastes. Fuel 2011;90:2585–91.
[14] Phanphanich M, Mani S. Impact of torrefaction on the grindability and fuel characteristics of forest biomass. Bioresour Technol 2011;102:1246–53.
[15] Repellin V, Govin A, Rolland M, Guyonnet R. Energy requirement for fine grinding of torrefied wood. Biomass Bioenergy 2010;34:923–30.
[16] Bridgeman TG, Jones JM, Shield I, Williams PT. Torrefaction of reed canary grass, wheat straw and willow to enhance solid fuel qualities and combustion properties. Fuel 2008;87:844–56.
[17] Pimchuai A, Dutta A, Basu P. Torrefaction of agriculture residue to enhance combustible properties. Energy Fuels 2010;24:4638–45.
[18] Deng J, Wang GJ, Kuang JH, Zhang YL, Luo YH. Pretreatment of agricultural residues for co-gasification via torrefaction. J Anal Appl Pyrolysis 2009;86:331–7.
[19] Hoekman SK, Broch A, Robbins C. Hydrothermal carbonization (HTC) of lignocellulosic biomass. Energy Fuels 2011;25:1802–10.
[20] Yan W, Hastings JT, Acharjee TC, Coronella CJ, Vasquez VR. Mass and energy balances of wet torrefaction of lignocellulosic biomass. Energy Fuels 2010;24:4738–42.
[21] Sarvaramini A, Gravel O, Larachi F. Torrefaction of ionic-liquid impregnated lignocellulosic biomass and its comparison to dry torrefaction. Fuel 2013;103:814–26.
[22] Prins MJ, Ptasinski KJ, Janssen F. Torrefaction of wood – Part 2. Analysis of products. J Anal Appl Pyrolysis 2006;77:35–40.
[23] Milne J L, Field C B. Assesment report from the GCEP workshop on energy supply with negative carbon emissions, 2012.
[24] Pronost J, Beaudoin G, Tremblay J, Larachi F, Duchesne J, Hebert R, et al. Carbon sequestration kinetic and storage capacity of ultramafic mining waste. Environ Sci Technol 2011;45:9413–20.
[25] Pronost J, Beaudoin G, Lemieux JM, Hebert R, Constantin M, Marcouiller S, et al. CO_2-depleted warm air venting from chrysotile milling waste (Thetford Mines, Canada): evidence for in-situ carbon capture from the atmosphere. Geology 2012;40:275–8.
[26] Bea SA, Wilson SA, Mayer KU, Dipple GM, Power IM, Gamazo P. Reactive transport modeling of natural carbon sequestration in ultramafic mine tailings. Vadose Zone J 2012;11.
[27] Wilson SA, Dipple GM, Power IM, Thom JM, Anderson RG, Raudsepp M, et al. Carbon dioxide fixation within mine wastes of ultramafic-hosted ore deposits: examples from the Clinton Creek and Cassiar chrysotile deposits. Canada Econ Geol 2009;104:95–112.
[28] Larachi F, Daldoul I, Beaudoin G. Fixation of CO_2 by chrysotile in low-pressure dry and moist carbonation: ex-situ and in-situ characterizations. Geochim Cosmochim Acta 2010;74:3051–75.
[29] Assima GP, Larachi F, Beaudoin G, Molson J. CO_2 Sequestration in chrysotile mining residues-implication of watering and passivation under environmental conditions. Ind Eng Chem Res 2012;51:8726–34.
[30] Assima GP, Larachi F, Beaudoin G, Molson J. Dynamics of carbon dioxide uptake in chrysotile mining residues-effect of mineralogy and liquid saturation. Int J Greenh Gas Control 2013;12:124–35.
[31] Channiwala SA, Parikh PP. A unified correlation for estimating HHV of solid, liquid and gaseous fuels. Fuel 2002;81:1051–63.
[32] Peng JH, Bi HT, Lim CJ, Sokhansanj S. Study on density, hardness, and moisture uptake of torrefied wood pellets. Energy Fuels 2013;27:967–74.
[33] Yang HP, Yan R, Chen HP, Lee DH, Zheng CG. Characteristics of hemicellulose, cellulose and lignin pyrolysis. Fuel 2007;86:1781–8.
[34] Sarvaramini A, Assima GP, Larachi F. Dry torrefaction of biomass – torrefied products and torrefaction kinetics using the distributed activation energy model. Chem Eng J 2013;229:498–507.
[35] Assima GP, Larachi F, Molson J, Beaudoin G. Accurate and direct quantification of native brucite in serpentine ores—new methodology and implications for CO_2 sequestration by mining residues. Thermochim Acta 2013;566:281–91.